J. Fluid Mech. (1996), *vol.* 318, *pp.* 107–128

Modal package convection in a porous layer with boundary imperfections

By D. N. RIAHI

Department of Theoretical and Applied Mechanics, 216 Talbot Laboratory, University of Illinois, Urbana, IL 61801, USA

(Received 22 January 1993 and in revised form 6 February 1996)

Thermal convection with a continuous finite bandwidth of modes in a porous layer with horizontal walls at different mean temperatures is considered when a spatially non-uniform temperature is prescribed at the lower wall. The nonlinear problem of three-dimensional convection for values of the Rayleigh number close to the classical critical value is solved by using multiple scales and perturbation techniques. The preferred flow solutions are determined by a stability analysis. It is found that for the case of near-resonant wavelength excitation regular or non-regular solutions in the form of superposition of small-scale multi-modal solutions with large-scale multi-modal (or non-modal) amplitude can become preferred, provided the wave vectors of the solutions are contained in the set of wave vectors due to the modal form of the boundary imperfections and the form of the large-scale part is the same as that due to the boundary imperfections. For the case of non-resonant wavelength excitation some three-dimensional solutions in the form of superposition of small-scale multi-modal solutions with large-scale multi-modal (or non-modal) amplitudes can be preferred, provided that the wavelength of the small-scale modulation is not too small. Large-scale flow structures are quite different from the small-scale flow structures in a number of cases and, in particular, they can exhibit kinks and can be non-modal in nature. The resulting flow patterns are affected accordingly, and they can provide quite unusual and non-regular three-dimensional preferred patterns. In particular, they are multiples of irregular rectangular patterns, and they can be non-periodic.

1. Introduction

Riahi (1993) investigated the problem of three-dimensional small-amplitude convection in a horizontal porous layer with a spatially non-uniform lower boundary temperature and for discrete modes only. The most surprising results were that regular or non-regular solutions in the form of multi-modal convection can become preferred in some range of the boundary modulation amplitude and wavenumber.

This paper extends the problem of discrete-modal convection at small amplitudes in a horizontal porous layer with lower boundary imperfections (Riahi 1993) to the case of convection with a continuous finite bandwidth of modes using the method of approach due to Newell & Whitehead (1969). As was explained in Newell & Whitehead (1969), such convective flow includes a wider class of solutions which can describe adequately problems with the amplitude modulations which inevitably occur as a result of, for example, non-uniform boundary imperfections.

Rees & Riley (1989*a*, *b*) investigated the effects of one-dimensional sinusoidal boundary imperfections on weakly nonlinear convection in a porous medium and determined, in particular, the nonlinear equations for the flow amplitudes, and the

effects of the boundary imperfections at the stability boundaries of different roll structures, and the evolution of the unstable rolls were studied.

The present problem, which is, in a sense, an extension of Rees & Riley's (1989*a*, *b*) work to two-dimensional imperfections and three-dimensional flows, is an example of an imperfect bifurcation driven by imperfect heating and/or cooling. The work of a number of authors is relevant to the present problem and this is reviewed in Riahi (1993).

The main purpose of the present study is to demonstrate the existence of some non-trivial and unusual results regarding the preferred flow solutions which can be realized near the onset of classical convection (Riahi 1983) because of the boundary imperfections, when a continuous band of modes is allowed to be represented. The main difference between the present work and Riahi (1993) is that here we treat modal packages instead of discrete modes, where the term modal package means a local continuous band of wavenumbers centred on a discrete mode (Newell & Whitehead 1969). The advantages of such an approach are discussed in detail in the latter reference.

The general problem under consideration can have practical value in that one might want to modulate the temperature of a boundary if the transport processes could be enhanced or if the flow structure could be controlled. The practical aspects of the problem and the main motivation for the study of the preferred convection pattern(s) were discussed in Riahi (1993).

The present investigation extends Riahi's (1993) problem to arbitrary three-dimensional modal package flows and an arbitrary one- or two-dimensional non-uniform temperature boundary condition in the form of a modal package at the lower wall. We have found a number of interesting results for both modal and non-modal envelope solutions. In particular, we found for the modal case that a non-regular small-scale flow solution with a regular or non-regular large-scale flow pattern can be preferred even if the spatially non-uniform boundary temperature represents a regular pattern. By a 'regular flow pattern' we mean a pattern of the flow solution whose wave vectors all have the same magnitudes and where the angles between the two consecutive wave vectors all have the same value. Superposition of two regular patterns is called a semi-regular pattern. A solution other than a regular and semi-regular one is called a non-regular solution. Examples of regular and non-regular flow patterns were given in Riahi (1993) and will not be repeated here. For non-modal envelope solution cases, we found stable non-periodic solutions with non-modal amplitudes where, depending on the form of the boundary imperfections, one such amplitude couplet in different parts of space may be 180° out of phase, and the solutions can exhibit kinks in the horizontal structure.

Let us denote the orders of magnitude of the amplitudes of convection and the non-uniform boundary temperature by ϵ and δ, respectively, where it is assumed that $\epsilon \ll 1$ and $\delta \ll 1$. Kelly & Pal (1978) investigated the two-dimensional discrete modal and non-trivial resonant wavelength excitation case where $\delta = O(\epsilon^3)$. They demonstrated (Kelly & Pal 1976, 1978) that this case corresponds to the range $R \approx R_c (R - R_c = O(\epsilon^2))$. Here R_c is the critical value of R (the Rayleigh number) below which there is no motion. For a discrete modal and non-resonant wavelength excitation case, Pal & Kelly (1978) applied a double series expansion in powers of δ and ϵ for each of the dependent variables and for R. Similar double series expansions were used by Rees & Riley (1989*b*). The present three-dimensional problem is based on some of the procedures used by Newell & Whitehead (1969), Kelly & Pal (1978), Pal & Kelly (1978) and Rees & Riley (1989*a*, *b*).

This paper starts with the formulation of the basic equations and the boundary conditions. The case of near-resonant wavelength excitation is considered in §3 and general, modal and non-modal analyses plus the results and some examples are provided there. The case of non-resonant wavelength excitation is correspondingly treated in §4. A general discussion with some comments about possible future extensions of the problem are given in §5, and §6 provides some brief conclusions from the results of the present study. Many of the equations, which can be quite lengthy, are not given in the present paper. They are, however, available from the author and can be provided to individual readers upon request.

2. Formulation

We consider an infinite horizontal porous layer of average depth d filled with fluid and heated from below. The layer is bounded above and below by two plane surfaces whose mean temperatures are $\bar{T}_u$ and $\bar{T}_l$, respectively. We choose to scale the temperature T^* on the basis of $\Delta T = \bar{T}_l - \bar{T}_u$. It is convenient to introduce a Cartesian system of coordinates, with the origin on the centreplane of the layer and with the z-coordinate in the vertical direction (opposite to the direction of the gravity force). We shall examine the effects of lower-boundary modulations at a fixed value of ΔT and represent the magnitude of such variation relative to ΔT by δ. We define a temperature relative to the conduction state by

$$T^*(x, y, z, t) = \left(\frac{d}{2} - z\right)\frac{\Delta T}{d} + T(x, y, z, t). \tag{2.1}$$

It is convenient to use non-dimensional variables in which lengths, velocities, time and temperature T are scaled respectively by d, $\lambda/d\rho_0 c$, $d^2\rho_0 c/\lambda$ and $\Delta T/R$. Here $R = \beta g K \Delta T d\rho_0 c/(\upsilon\lambda)$ is the Rayleigh number, β is the coefficient of thermal expansion, g is the acceleration due to gravity, K is the Darcy permeability coefficient, ρ_0 is the reference fluid density, c is the specific heat at constant pressure, λ is the thermal conductivity of the porous medium (fluid–solid mixture) and υ is the kinematic viscosity. Then, with the usual Boussinesq approximation that density variations are taken into account only in the buoyancy term, the Darcy–Boussinesq–Oberbeck equations for momentum, continuity and heat in the limit of infinite Prandtl–Darcy number (Joseph 1976) are obtained, which are given in Riahi (1993). These are equations for θ, $\boldsymbol{u}$ and p. Here θ is dimensionless T, $\boldsymbol{u}$ is the velocity vector and p is the modified deviation of pressure from its static value.

The governing equations are simplified by using the representation

$$\boldsymbol{u} = \boldsymbol{\Omega}\phi, \quad \boldsymbol{\Omega} \equiv \nabla x \cdot \nabla x \boldsymbol{z}, \tag{2.2}$$

for the divergence-free velocity vector field $\boldsymbol{u}$ (Riahi 1983). Here $\boldsymbol{z}$ is a unit vector in the vertical direction and ϕ is the poloidal function for $\boldsymbol{u}$.

Taking the vertical component of the double curl of the momentum equation and using (2.2) in the heat equation yields the following equations:

$$\Delta_2(\nabla^2\phi + \theta) = 0, \tag{2.3a}$$

$$\left(\nabla^2 - \frac{\partial}{\partial t}\right)\theta - R\Delta_2\phi = \boldsymbol{\Omega}\phi \cdot \nabla\theta, \tag{2.3b}$$

where

$$\Delta_2 = \frac{\partial^2}{\partial x^2} + \frac{\partial^2}{\partial y^2}.$$

Equation (2.3) must then be solved subject to the boundary conditions

$$\phi = 0 \quad \text{at} \quad z = \pm\tfrac{1}{2}, \tag{2.4a}$$

$$\theta = \delta R h(x, y) \quad \text{at} \quad z = -\tfrac{1}{2}, \tag{2.4b}$$

$$\theta = 0 \quad \text{at} \quad z = \tfrac{1}{2}, \tag{2.4c}$$

where $h(x, y)$ is a given spatially non-uniform function of x and y.

3. Near-resonant wavelength excitation

3.1. *General analysis*

This case corresponds to the critical regime where $R \approx R_c$ and $\delta = O(\epsilon^3)$ (Kelly & Pal 1978). We consider the following expansions for ϕ, θ and R in powers of ϵ:

$$\begin{pmatrix} \phi \\ \theta \\ R \end{pmatrix} = \begin{pmatrix} 0 \\ 0 \\ R_0 \end{pmatrix} + \epsilon \begin{pmatrix} \phi_1 \\ \theta_1 \\ R_1 \end{pmatrix} + \epsilon^2 \begin{pmatrix} \phi_2 \\ \theta_2 \\ R_2 \end{pmatrix} + \ldots \tag{3.1}$$

and set $\delta = \epsilon^3$. Upon inserting (3.1) into (2.3) and (2.4) and disregarding the quadratic terms, we find the linear problem, whose system of equations is given in Riahi (1993). This system is the classical linear system (Riahi 1983) whose general modal package solution can be written as

$$\begin{pmatrix} \phi_1 \\ \theta_1 \end{pmatrix} = \begin{pmatrix} f(z) \\ g(z) \end{pmatrix} \sum_{n=-N}^{N} W_n(x, y)\, A_n(x_s, y_s, t_s), \tag{3.2}$$

where A_n are functions of the flow variables

$$x_s = \epsilon x, \quad y_s = \epsilon^{1/2} y, \quad t_s = \epsilon^2 t \tag{3.3}$$

(Newell & Whitehead 1969). This scaling restricts the analysis to perturbations from two-dimensional roll solutions. The function W_n introduced in (3.2) has the representation

$$W_n \equiv \exp(\mathrm{i}\boldsymbol{k}_n \cdot \boldsymbol{r}), \tag{3.4a}$$

and satisfies the relation

$$-\Delta_2 W_n = \alpha^2 W_n. \tag{3.4b}$$

Here $\boldsymbol{r}$ is the horizontal position vector, $\mathrm{i} = \sqrt{-1}$, α is the horizontal wavenumber of the flow structure, N is a positive integer, and the horizontal wavenumber vectors $\boldsymbol{k}_n = (k_{nx}, k_{ny})$ of the flow structure satisfy the properties

$$\boldsymbol{k}_n \cdot \boldsymbol{z} = 0, \quad |\boldsymbol{k}_n| = \alpha, \quad \boldsymbol{k}_n = -\boldsymbol{k}_n. \tag{3.5}$$

The amplitude functions A_n satisfy the condition

$$A_n^* = A_{-n}, \tag{3.6}$$

where the asterisk indicates the complex conjugate. Following Riahi (1983), the results for R_0, its minimum R_c attained at $\alpha = \alpha_c$, and the expressions for $f(z)$ and $g(z)$ are obtained; they are given in Riahi (1993).

At order ϵ^2, (2.3) and (2.4) become a system of the classical type (Riahi 1983), except for the terms which are due to variations of ϕ_1 and θ_1 with respect to slow variables in the present formulation.

Since the classical problem is self-adjoint, the solvability conditions for the equations

of higher order in ϵ require us to define the following special solutions ϕ_{1n} and θ_{1n} of the linear system:

$$\begin{pmatrix}\phi_{1n}\\ \theta_{1n}\end{pmatrix} = \begin{pmatrix}f(z)\\ g(z)\end{pmatrix} W_n. \tag{3.7}$$

Multiplying (2.3*a*) by ϕ_{1n}^*, (2.3*b*) by $-R_0^{-1}\theta_{1n}^*$, adding and averaging over the whole layer (in x, y and z) and using the boundary conditions (2.4) yields $R_1 = 0$ at order ϵ^2 (Riahi 1983). At order ϵ^3, (2.3) and (2.4) involve the function h which is assumed to have the following arbitrary representation:

$$h(x,y) = R_c^{-1} \sum_{n=-N^{(b)}}^{N^{(b)}} L_n W_n^{(b)} \equiv R_c^{-1} \sum_{n=-N^{(b)}}^{N^{(b)}} L_n \exp(\mathrm{i}\boldsymbol{k}_n^{(b)}\cdot\boldsymbol{r}), \tag{3.8}$$

where L_n are functions of x_s and y_s, $N^{(b)}$ is a positive integer which may tend to infinity, and the horizontal wavenumber vectors $\boldsymbol{k}_n^{(b)} = (k_{nx}^{(b)}, k_{ny}^{(b)})$ satisfy the properties,

$$\boldsymbol{k}_n^{(b)}\cdot\boldsymbol{z} = 0, \quad |\boldsymbol{k}_n^{(b)}| = \alpha_n^{(b)}, \quad \boldsymbol{k}_n^{(b)} = -\boldsymbol{k}_n^{(b)}. \tag{3.9}$$

The functions L_n satisfy the condition

$$L_n^* = L_{-n}. \tag{3.10}$$

We shall assume that $\alpha_n^{(b)} = \alpha_c = \pi$ (Riahi 1983). In general, $\alpha_n^{(b)}$ are not all the same as α_c for different n. Most of these latter cases will be considered in §4, while the rest will be discussed in §5.

Multiplying (2.3*a*) by ϕ_{1n}^*, (2.3*b*) by $-R_0^{-1}\theta_{1n}^*$, adding and averaging over the whole layer (in x, y and z) and using the boundary conditions (2.4) yields a system of equations for A_n ($n = -N, \ldots, -1, 1, \ldots, N$) at order ϵ^3. This system also contains R_2. Hereafter, angular brackets indicate an average over the fluid layer.

Using the above results, doing some scalings of t_s, L_m and A_m (for all possible m) and applying the conditions given in Riahi (1993) for the non-zero average product $\langle W_n^* W_1 W_p Wm\rangle$, we end up with the simplified form of the above system which we refer to here as system (A). System (A) is also a collection of $2N$ partial differential equations for the $2N$ unknown functions A_n ($n = -N, \ldots, -1, 1, \ldots, N$).

To distinguish the physically realizable solution(s) among all the steady solutions of (A), the stability of A_m ($m = -N, \ldots, -1, 1, \ldots, N$) with respect to disturbances $B_m(x_s, y_s, t_s)$ are investigated. The system of equations for the time-dependent disturbances $B_n(n = -N, \ldots, -1, 1, \ldots, N)$ with the addition of a time dependence of the form $\exp(\sigma t_s)$ is then considered. The disturbance amplitude functions B_n satisfy conditions of the form (3.6) for $\sigma = \sigma^*$. Taking the complex conjugate of the disturbance system and replacing the subscript n by $-n$, it then can be seen after some re-arrangement that $B_n \exp(\sigma t_s) = B_{-n}^* \exp(\sigma^* t_s)$ which implies that σ is real. It is clear that the modulation affects the steady solutions directly as source terms in (A) while the modulation affects the disturbances indirectly through the steady solutions.

3.2. *Modal analysis*

The functions $L_m(x_s, y_s)$ given in (A) are assumed to have the following arbitrary representations:

$$L_m(x_s, y_s) = \sum_{n=-M^{(b)}}^{M^{(b)}} l_{mn}\, \nu_{nm}^{(b)} \equiv \sum_{n=-M^{(b)}}^{M^{(b)}} l_{mn} \exp(\mathrm{i}\boldsymbol{y}_{nm}^{(b)}\cdot\boldsymbol{r}_s)$$
$$(m = -N^{(b)}, \ldots, -1, 1, \ldots, N^{(b)}), \tag{3.11}$$

where $M^{(b)}$ is a positive integer which may tend to infinity, $\boldsymbol{r}_s = (x_s, y_s)$, the horizontal wavenumber vectors $\gamma_{nm}^{(b)} = (\gamma_{nmx}^{(b)}, \gamma_{nmy}^{(b)})$ satisfy the properties

$$\gamma_{nm}^{(b)} \cdot \boldsymbol{z} = 0, \quad |\gamma_{nm}^{b}| = \lambda_{nm}^{(b)}, \quad \gamma_{-nm}^{(b)} = -\gamma_{nm}^{(b)}, \quad \gamma_{n,-m}^{(b)} = -\gamma_{nm}^{(b)}, \tag{3.12}$$

and the constant coefficients l_{mn} satisfy the condition

$$l_{mn}^{*} = l_{-mn}. \tag{3.13}$$

For $L_m = 0$ or $\langle W_n^* W_m^{(b)} \rangle = 0$ $(m = -N^{(b)}, \ldots, -1, \ldots, N^{(b)})$, the expressions for R_2 and σ given by (A) and the disturbance system are the same as the corresponding ones for the classical problem in the absence of modulation. The wavenumbers $\lambda_{nm}^{(b)}$ are all assumed to have the same values as $\lambda^{(b)}$.

The system (A) and the representation (3.11) for significant modulation suggest assuming the following steady form for A_n:

$$A_n(x_s, y_s) = \sum_{j=-M}^{j=M} a_{nj} \nu_{jn}(x_s, y_s), \tag{3.14a}$$

$$\nu_{jn} = \exp(\mathrm{i}\gamma_{jn} \cdot \boldsymbol{r}_s), \tag{3.14b}$$

where M is a positive integer, and the wave vectors γ_{jn} satisfy properties of the type (3.12) with no superscript b. We shall assume that the wavenumbers λ_{nm} all have the same value as λ.

Using (3.11) and (3.14) in (A), multiplying the system (A) by $\nu_{n'n}^*$ and averaging over the slow variables (x_s and y_s), we end up with a lengthy system for the coefficients $a_{nn'}$.

The form (3.14) of the steady solutions A_n suggests that the disturbance amplitude function B_n, obeyed by the disturbance system, should be of the form

$$B_n(x_s, y_s) = \sum_{j=-\infty}^{\infty} b_{nj} \tilde{\nu}_{jn}(x_s, y_s), \tag{3.15a}$$

where

$$\tilde{\nu}_{jn} \equiv \exp(\mathrm{i}\tilde{\gamma}_{jn} \cdot \boldsymbol{r}_s). \tag{3.15b}$$

The horizontal wavenumber vectors $\tilde{\gamma}_{nm} = (\tilde{\gamma}_{nmx}, \tilde{\gamma}_{nmy})$ of disturbances satisfy the properties

$$\tilde{\gamma}_{j(-n)} = \tilde{\gamma}_{jn}, \quad \tilde{\gamma}_{nm} \cdot \boldsymbol{z} = 0, \quad |\tilde{\gamma}_{nm}| = \lambda_{nm}, \quad \tilde{\gamma}_{(-n)m} = -\tilde{\gamma}_{nm}, \quad \tilde{\gamma}_{nm} \equiv \gamma_{nm}$$
$$(\text{for } n = -M^{(b)}, \ldots, -1, 1, \ldots, M^{(b)};\ m = -N, \ldots, -1, \ldots, N). \tag{3.16}$$

The constant coefficients b_{nj} satisfy the condition

$$b_{-nj} = b_{nj}^{*}. \tag{3.17}$$

Using (3.14) and (3.15) in the disturbance system, multiplying this by $\tilde{\nu}_{n'n}^*$ and averaging over the slow variables, we find a lengthy system for the coefficients $b_{nn'}$. It is seen from (3.14) and (3.15) that the wave vectors of the steady amplitudes are the same as those of the boundary modulation, while the wave vectors of the disturbance amplitudes contain those of the boundary modulation. The preferred solution corresponds to the one for which σ from the system for $b_{nn'}$ is non-positive and R_2 from the system for $\alpha_{nn'}$ is the smallest among all the stable solutions.

Note that (3.14)–(3.17) and the systems for $a_{nn'}$ and $b_{nn'}$ are based on the assumption that at least one wave vector $\boldsymbol{k}_n$ of the flow coincides with one wave vector $\boldsymbol{k}_m^{(b)}$ of the boundary modulation. This is the non-trivial case which we refer to as the significant modulation case, since otherwise the boundary modulation is ineffective.

The systems for $a_{nn'}$ and $b_{nn'}$ are then simplified by evaluating the average products of the type $\langle W_n^* W_l W_p W_m \rangle$, etc.

Let us now consider the following specific examples in order to illustrate the non-trivial and often surprising inter-relations between the boundary modulation pattern and the subsequent preferred flow pattern.

Example 1

$M = M^{(b)} = N^{(b)} = 1$, $A_n = a_{nl}\nu_{ln}$ and real a_{nl}. Consider the case $N = 1$ first. The expression (3.14) for A_n then implies that $a_{n,-1} = 0$, and A_n is complex. Using (3.6), we find that $a_{n1} = a_{-n,1}$ since a_{n1} is real. For $n' = -1$, the system for $a_{nn'}$ implies $l_{n,-1} = 0$, while for a significant corrugation effect ($\gamma_{n'n} = \gamma^{(b)}_{m'n}$ and $\boldsymbol{k}_1 = \boldsymbol{k}^{(b)}_m$) and for $n' = -1$ it leads to the following equation for a_{nl}:

$$a_{nl}^3 + (\beta_{nl}/2)\, a_{nl} - l_{nl}/2 = 0, \tag{3.18a}$$

where

$$\beta_{nn'} \equiv -R_2 + \left(\gamma_{n'nx} + \frac{\gamma^2_{n'ny}}{2k_{nx}}\right)^2. \tag{3.18b}$$

The above equation implies that l_{n1} should also be real. Since $a_{nl} = a_{-n,l}$, (3.18) implies that

$$l_{-1,1} = l_{11} + (\beta_{-1,1} - \beta_{11})\, a_{11}. \tag{3.19}$$

We assume that (3.19) holds. Defining

$$r_{nl} = \tfrac{1}{4} l_{nl}, \quad \Gamma_{nl} = \tfrac{1}{6}\beta_{nl}, \quad D_{nl} = \Gamma^3_{nl} + r^2_{nl}, \tag{3.20}$$

we find that there is only one real root for (3.18a) if

$$R_2 < \left(\gamma_{1nx} + \frac{\gamma^2_{1ny}}{2k_{nx}}\right)^2 + (\tfrac{27}{2})^{1/3} |l_{nl}|^{2/3}, \tag{3.21}$$

while there are three real roots otherwise, and that

$$a_{nl} = [r_{nl} + D^{1/2}_{nl}]^{1/3} + [r_{nl} - D^{1/2}_{nl}]^{1/3} \tag{3.22}$$

for the case where (3.21) holds. Since the preferred solution corresponds to the smallest value of R_2, (3.22) is the only real root of (3.18a) and is the preferred solution. Next, we consider the stability of (3.22). For $|n'| > 1$, the system for $b_{nn'}$ yields the result that $b_{nn'} (n = -1, 1)$ are real and satisfy the following equations:

$$(\sigma + \beta_{-1n'} + 7a^2_{11})\, b_{-1n'} + 2a^2_{11}\, b_{1n'} = 0, \tag{3.23a}$$

$$2a^2_{11}\, b_{-1n'} + (\sigma + \tilde{\beta}_{1n'} + 7a^2_{11})\, b_{1n'} = 0, \tag{3.23b}$$

where

$$\tilde{\beta}_{nn'} = -R_2 + \left(\tilde{\gamma}_{n'nx} + \frac{\tilde{\gamma}^2_{n'ny}}{2k_{nx}}\right)^2. \tag{3.24}$$

Applying the condition for non-trivial solution for (3.23) leads to a quadratic equation for σ whose roots are real. For sufficiently large $|R_2|$ this equation has at least one positive root for $R_2 > 0$, while both roots are negative for $R_2 < 0$. Hence the preferred solution a_{n1} which corresponds to the smallest value of R_2 is indeed stable with respect to disturbances for which $|n'| > 1$. For $|n'| < 1$ the system for $b_{nn'}$ yields the result that σ is real and that these disturbances are less dangerous than those for the $|n'| > 1$ case.

We now consider the case of arbitrary $N > 1$. For $1 < n \leqslant N$, the system for $a_{nn'}$ yields the following non-trivial equation for $a_{nn'}$:

$$\left[\beta_{nn'} - 2a^2_{nn'} + 2\sum_{m=1}^{m=N} c_{mn}\, a^2_{mm'}\right] a_{nn'} = 0, \tag{3.25a}$$

where

$$c_{mn} \equiv (2 + \Psi_{mn} + \Psi_{-mn})/2, \tag{3.25b}$$

and Ψ_{mn} is defined by

$$\Psi_{mn} = (3-\hat{\phi}_{mn})(1+\hat{\phi}_{mn})^2/(7-4\hat{\phi}_{mn}+\hat{\phi}_{mn}^2), \quad \hat{\phi}_{mn} \equiv \alpha^{-2}(\boldsymbol{k}_m \cdot \boldsymbol{k}_n). \quad (3.25c)$$

This equation implies that there exists a non-trivial solution only if $\beta_{nn'} < 0$ for values of n for which $a_{nn'} \neq 0$ since $\Psi_{mn} + \Psi_{-mn} > 0$. However, a negative value of $\beta_{nn'}$ defined by (3.18) implies that $R_2 > 0$ for arbitrary $N > 1$. Hence solutions for $N > 1$ are not preferred compared to the one for $N = 1$ which corresponds to $R_2 < 0$. The results discussed above indicate that small-scale two-dimensional rolls solutions along the corrugation wave vector $\boldsymbol{k}_1^{(b)}$ with large-scale roll amplitudes along $\gamma_{1n}^{(b)}$ are, thus, preferred. The resulting flow pattern with $\boldsymbol{k}_1^{(b)} + \epsilon\gamma_{11}^{(b)}$ along the x-axis becomes rolls parallel to the y-axis. Streamlines in the (x, y)-plane are thus straight lines parallel to the y-axis. Similarly, the lower-boundary isothermal lines are all straight lines parallel to the y-axis. The flow pattern of the solution (streamlines) projected on the vertical (x, z)-plane is also determined for $\alpha = \alpha_1^{(b)} = \lambda = \lambda^{(b)} = \pi$ and $\epsilon = 0.1$. Clearly the preferred flow pattern in this case has a wavelength slightly larger than the one from classical theory (Riahi 1983), but the horizontal flow structure follows the boundary imperfection shape. The roll cells in this case also repeat themselves along x-axis.

Example 2

This example is essentially the same as the previous one, except that now $A_n = a_{n1}\nu_{1n} + a_{n,-1}\nu_{-1,n}$ for real a_{n1} and $a_{n,-1}$. We assume real l_{mn} and take the case $l_{11} = l_{1,-1}$. Using the same procedure as in example 1, we find that the preferred solution corresponds to the case of significant corrugation effects and $N = 1$. The following equation for $a_{nn'}$ then results from the system for $a_{nn'}$:

$$2a_{nn'}^3 + (8+\beta_{nn'})\,a_{nn'} - \sum_{m,\,m'=-1}^{1} l_{mm'} = 0. \quad (3.26)$$

We assume that $\gamma_{nn'}^{(b)}$ is either along the x-axis or along the y-axis which implies that $\beta_{n1} = \beta_{n,-1}$. For $R_2 < 0$, $\beta_{nn'} > 0$ and there is only one real root to equation (3.26) for $a_{nn'}$. We find that $a_{nn'} = a_{11}$ for $n, n' = -1, 1$. The resulting isothermal lines at the lower boundary and the flow streamlines in the (x, y)-plane are shown in figures 1(*a*) and 1(*b*) for the case of $\boldsymbol{k}_1^{(b)}$ parallel to the x-axis, $\gamma_{11}^{(b)}$ parallel to the y-axis, and for $\epsilon = 0.1, \lambda = \lambda^{(b)} = 9.1\pi, \alpha = \alpha_n^{(b)} = \pi$. It is seen from these figures that the preferred flow pattern is due to rectangular cells with the wavelength along the y-axis somewhat larger than the one along the x-axis. The isotherms also exhibit a rectangular pattern and with the wavelength along the y-axis larger than the one along the x-axis. Again as in example 1, the cells are repeatable along both the x- and y-axes. The patterns shown in figures 1(*a*) and 1(*b*) have a horizontal wavenumber of about $1.35\alpha_c$, and they have the same wavelength along the x- and y-directions. All the figures herein are drawn at $O(1)$ scales.

Example 3

$M = M^{(b)} = 1$, $N^{(b)} = 2$, $A_n = a_{n1}\nu_{1n}$ and real a_{n1}. Expression (3.14) for A_n implies that $a_{n,-1} = 0$ and A_n is complex. Using (3.6), we find that $a_{n1} = a_{-n1}$ since a_{n1} is real. Consider first $N = 1$. For $n' = -1$, the system for $a_{nn'}$ implies $l_{n,-1} = 0$, while for significant corrugation effect ($\gamma_{n'n} = \gamma_{m'n}^{(b)}$ and $\boldsymbol{k}_n = \boldsymbol{k}_m^{(b)}$) and for $n' = 1$ it leads to equation (3.21*a*) for $N = 1$. The results (3.19)–(3.23) for $N = 1$ then follow.

For $N = 2$, the system for $a_{nn'}$ leads to the following non-trivial equations for a_{11} and a_{21}:

$$[\beta_{11} + 2c_{21}\alpha_{21}^2]\,\alpha_{11} = l_{11} - 2\alpha_{11}^3, \quad [\beta_{21} + 2c_{21}a_{21}^2]\,a_{21} = l_{21} - 2a_{21}^3. \quad (3.27a, b)$$

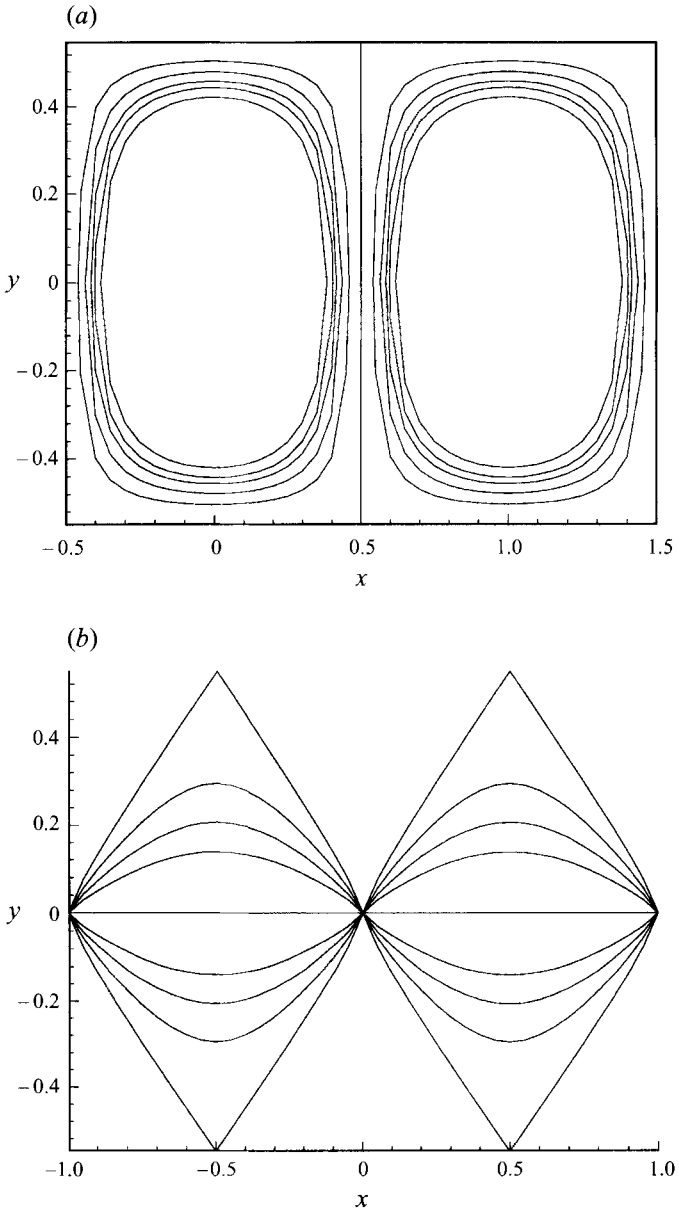

FIGURE 1. (*a*) Isothermal lines at the lower boundary and (*b*) streamlines in the (x, y)-plane, with $\boldsymbol{k}_1^{(b)}$ parallel to the x-axis, $\gamma_{11}^{(b)}$ along the y-axis and for $M = M^{(b)} = N = N^{(b)} = 1, A_n = a_{n1} v_{1n} + a_{n,-1} v_{-1,n}$ (real a_{n1} and $a_{n,-1}$), $\epsilon = 0.1, \boldsymbol{k}_n = \boldsymbol{k}_n^{(b)} \gamma_{1n} = \gamma_{1n}^{(b)}, \alpha = \alpha_n^{(b)} = \pi, \lambda = \lambda^{(b)} = 9.1\pi$.

The preferred solutions to (3.27) correspond to the case where there is only a single real root. The range for R_2 for which these solutions exist is wider than for $N = 1$.

Next, we consider the general $N > 2$ case. There exists at least one n such that the system for $a_{nn'}$ leads to the following non-trivial equation for the coefficients $a_{m1} (m = 1, \ldots, N)$:

$$6a_{nl}^2 = -\sum_{m=1}^{m=N} 2c_{mn} a_{ml}^2 - \beta_{nl}. \tag{3.28}$$

Since $a_{m1}(m = 1, \ldots, N)$ are all real, (3.28) implies that β_{n1} defined by (3.18b) should be negative which means that R_2 should be positive. Hence, such solutions are not preferred compared to the cases $N = 1, 2$ which can correspond to sufficiently small and negative R_2 and are possible preferred solutions for this example. Stability analysis for the cases $N = 1, 2$ based on the system for $b_{nn'}$ also indicates that the solutions for these two cases are stable for sufficiently small and negative values of R_2. The preferred flow solution, thus, can be small-scale rectangles or a roll solution with large-scale roll amplitude. The problem can also be generalized to arbitrary $N^{(b)}$. All solutions for $N \leqslant N^{(b)}$ are possible preferred solutions for sufficiently small and negative R_2, while solutions for $N > N^{(b)}$ are not preferred since they correspond to positive R_2. The preferred flow patterns, thus, can be superimposed small-scale multi-modal ($N \leqslant N^{(b)}$) solution with large-scale roll amplitude. The resulting isotherms at $z = -\frac{1}{2}$ and the flow streamlines in the (x, z)- and (x, y)-planes are determined explicitly for $N = 2$ and for $\boldsymbol{k}_1^{(b)} + \epsilon \boldsymbol{\gamma}_{11}^{(b)}$ parallel to the x-axis, $\mathrm{k}_2^{(b)} + \epsilon \boldsymbol{\gamma}_{12}^{(b)}$ along the y-axis, and for $|\boldsymbol{k}_1^{(b)} + \epsilon \boldsymbol{\gamma}_{11}^{(b)}| = 1.1\pi$, $|\boldsymbol{k}_2^{(b)} + \epsilon \boldsymbol{\gamma}_{12}^{(b)}| = 0.9\pi$. It is found from these results that the preferred horizontal flow pattern is rectangular with wavelength along the y-axis slightly larger than the one along the x-axis and is similar to that shown in figure 1 (b). The vertical structure of the preferred flow pattern is also rectangular and is slightly longer along the z-axis. The isotherms also exhibit a rectangular shape similar to those shown in figure 1 (a). The horizontal wavenumber of the preferred flow is about $1.42\alpha_c$.

Example 4

$M = M^{(b)} = 2$, $N^{(b)} = 1$, $A_n = (a_{n1} \nu_{1n} + a_{n2} \nu_{2n})$ and real a_{n1} and a_{n2}. Here again $a_{n,-1} = a_{n,-2} = 0$, A_n is complex and $a_{ni} = a_{-ni} (i = 1, 2)$. Consider $N = 1$ first. The system for $a_{nn'}$ leads to the following simplified equations for a_{n1} and a_{n2}:

$$(\beta_{n1} + 6a_{n2}^2)\, a_{n1} = l_{n1} - 2a_{n1}^3, \quad (\beta_{n2} + 6a_{n1}^2)\, a_{n2} = l_{n2} - 2a_{n2}^3. \tag{3.29a, b}$$

The preferred solutions to (3.29) correspond to the case where there is only a single real root. The range for R_2 for which these solutions exist is wider than the corresponding case for $M^{(b)} = 1$.

Next, we consider the general $N > 1$ case. There exists at least one n such that the system for $a_{nn'}$ leads to the following non-trivial equations for a_{n1} and a_{n2}:

$$\beta_{n1} a_{n1} = -\sum_{m=-N}^{m=N} (1 + \Psi_{mn})\, a_{n1} (a_{m1} + a_{m2})^2 + 2a_{n1}(a_{n1}^2 + 3a_{n2}^2) + 2 \sum_{m=-N}^{m=N} (1 + \Psi_{mn})(a_{n1} - a_{n2})\, a_{m1} a_{m2}, \tag{3.30a}$$

$$\beta_{n2} a_{n2} = -\sum_{m=-N}^{m=N} (1 + \Psi_{mn})\, a_{n2} (a_{m1} + a_{m2})^2 + 2a_{n2}(a_{n2}^2 + 3a_{n1}^2) - 2 \sum_{m=-N}^{m=N} (1 + \Psi_{mn})(a_{n1} - a_{n2})\, a_{m1} a_{m2}. \tag{3.30b}$$

It is seen that (3.30b) can be derived from (3.30a) by replacing subscript $n1$ by $n2$. Hence, results for general N can be obtained by considering the case $a_{n1} = a_{n2}$ and $\beta_{n1} = \beta_{n2}$ for the particular n under consideration. Then, (3.30) implies that there exists a non-trivial solution only for positive R_2. Hence these solutions for $N > 1$ are not preferred. The preferred flow solution, thus, can be small-scale roll solution with the large-scale rectangular form of amplitude.

The resulting isotherms at $z = -\frac{1}{2}$ and the flow streamlines in the (x, y)-plane are calculated for $N = 1$ and for real l_{nm}, $l_{n1} = l_{n2}$, $l_{n,-2} = l_{n,-1} = 0$, $\boldsymbol{k}_1^{(b)} + \epsilon\boldsymbol{\gamma}_{11}^{(b)}$ parallel to the x-axis, $\boldsymbol{k}_1^{(b)} + \epsilon\boldsymbol{\gamma}_{21}^{(b)}$ parallel to the y-axis, and for $|\boldsymbol{k}_1^{(b)} + \epsilon\boldsymbol{\gamma}_{11}^{(b)}| = 1.1\pi$, $|\boldsymbol{k}_1^{(b)} + \boldsymbol{\gamma}_{21}^{(b)}| = 1.1\pi$. It is found from these results that the preferred horizontal flow is essentially in the form of square pattern. The isotherms also exhibit a similar pattern. The horizontal wavenumber of the preferred flow is about 1.56π.

The four examples presented above can be generalized to the case of arbitrary $N^{(b)}$, arbitrary $M^{(b)}$,

$$A_n = \sum_{n'=1}^{n'=M} a_{nn'} v_{n'n}$$

with real $a_{nn'}$ and $M = M^{(b)}$. The preferred flow solution is the superposition of a small-scale multi-modal ($N \leqslant N^{(b)}$) solution and a large-scale multi-modal ($N \leqslant M^{(b)}$) amplitude function.

3.3. *Non-modal analysis*

We consider the amplitude system (A) for cases where

$$A_n = a_n \tanh x_s + \mathrm{i} b_n \operatorname{sech} x_s = \bar{u}_n + \mathrm{i}\bar{v}_n, \tag{3.31}$$

where $\bar{u}_n$ and $\bar{v}_n$ are the real and imaginary parts of A_n, respectively. Equation (3.31) is suggested by the simple envelope solution due to Newell & Whitehead (1969) in their studies of finite-bandwidth finite-amplitude roll convection. The coefficients a_n and b_n given in (3.31) are real constants. Equation (3.31) is suggested by the following form of the boundary imperfection functions L_m:

$$L_m = g_m \tanh x_s + \mathrm{i} h_m \operatorname{sech} x_s, \tag{3.32}$$

where g_m and h_m are real constants. The justification for such a choice was confirmed by using (3.31) and (3.32) in (A) which leads to an algebraic system of $8N$ equations for $4(N + N^{(b)})$ unknown coefficients a_m, b_m, g_m and h_m. Generally, a solution for $N > N^{(b)}$ is not possible, unless $a_m = b_m = 0$ for $m > N^{(b)}$. Non-trivial solutions ($a_m \neq 0$, $b_m \neq 0$) are always possible for $N \leqslant N^{(b)}$. Of course we are assuming significant boundary imperfections, so that the above system involves at least one non-zero g_m or h_m.

It should be noted that one could, in general, consider any solution of the form $A_n = F_n(x_s, y_s)$ for (A), for given functions F_n, where the functions L_m are chosen to satisfy (A). However, detailed investigation of the stability of such a solution requires knowledge of particular forms of F_n, although as we shall see later in this subsection, all such types of solution can become stable for sufficiently large $|R_2|$ and $R_2 < 0$, provided the horizontal averages of functions involving the base flow and disturbance quantities and/or their first or higher derivatives remain finite.

Before considering the stability of solutions of the form (3.31), it is worth stating that one of the main reasons for assuming this form of solutions is the rather unusual non-modal properties of the real parts $\bar{u}_n$ of such solutions. Where u_n is weak, namely at $x_s = 0$, $\bar{v}_n$ is stronger and vice versa. For large $|x_s|$, the solutions (3.2) are of scale $2\pi/\alpha_c$ but the sense of rotation of the corresponding pattern couplets due to $\bar{u}_n$ is reversed on the opposite side of the $x_s = 0$ axis.

Next, we consider stability of solutions of the form (3.31) with respect to disturbances B_n of the general form

$$B_n = \hat{u}_n + \mathrm{i}\hat{v}_n, \tag{3.33}$$

where $\hat{u}_n$ and $\hat{v}_n$ are the real and imaginary parts of B_n, respectively. Using (3.31) and

(3.33) in the disturbance system and separating the real and imaginary parts leads us to systems for $\hat{u}_n$ and $\hat{v}_n$. Multiply the system for $\hat{u}_n$ by $\hat{u}_n$, that for $\hat{v}_n$ by $\hat{v}_n$, add the two results and average over the slow variables. The resulting system has the property that $\sigma < 0$ for sufficiently large $|R_2|$ and $R_2 < 0$, provided the resulting horizontal averages which involve $\bar{u}_n, \bar{v}_n, \hat{u}_n, \hat{v}_n$ and their first- or higher-order derivatives remain finite. This result holds for general base flow solutions which include those in (3.31), provided that the boundary imperfections are significant so that at least one $\boldsymbol{k}_n$ is along one $\boldsymbol{k}_m^{(b)}$. For insignificant boundary imperfections, where none of the wave vectors $\boldsymbol{k}_n$ are along any of the wave vectors $\boldsymbol{k}_m^{(b)}$, it is not difficult to show from the systems for (a_n, b_n) and $(\hat{u}_n, \hat{v}_n)$ that the base flow solutions with 'kinks' $\bar{u}_n = a \tanh x_x$ and $\bar{v}_n = 0$ for all n are unstable and $R_2 = 2$ and $\sigma = 1$ follow. For significant boundary imperfections, such solutions can be stable as the following examples indicate. In particular, a solution to the problem presented in example 1 given below for $N = N^{(b)} = 1$, $R_2 < 0$, $h_1 = 0$ and with the amplitude function given by (3.31) with $b_1 = 0$ is stable, provided $a_1 = \sqrt{2}$ for $g_1 > 0$ or $a_1 = -\sqrt{2}$ for $g_1 < 0$. Such a stable solution for this problems turn out to be also the preferred one, compared to other possible stable solutions with $b_1 \neq 0$, since it corresponds to smaller R_2, as the details presented in the example 1 below indicate. The boundary imperfection corresponding to such a stable solution has the following form for the shape function h, given by (3.8):

$$h = 2R_c^{-1} g_1 \tanh x_s \cos(\boldsymbol{k}_1^{(b)} \cdot \boldsymbol{r}),$$

which has the same horizontal variations as the one for the temperature deviation θ_1 or the poloidal velocity component ϕ_1 of the stable solution for a significant imperfection ($\boldsymbol{k}_1 = \boldsymbol{k}_1^{(b)}$). The reason for the stabilization of such a solution lies on the fact that this is a near-resonant case and that the wave vector of the solution is parallel to the imperfection wave vector. The stability analysis for such a solution indicated that only under the above conditions on g_1, h_1, a_1, b_1 and R_2 is such solution stable with respect to disturbances of the form (3.33).

Let us now consider the following specific examples in order to illustrate the interrelations between the boundary imperfections and the resulting preferred flow patterns and to demonstrate specific conditions on R_2 under which the absolute stability of different solutions with 'kinks' is possible.

Example 1

$N^{(b)} = 1$. Consider the case $N = 1$ first. Suppose $g_1 = 0$ and $h_1 \neq 0$. Then the system for a_n and b_n implies that both a_1 and b_1 are non-zero and $R_2 = 2(1 + h_1^2)$. Assuming that the disturbance quantities $\hat{u}_1$ and $\hat{v}_1$ have a dependence on y_s of the form $\exp(\beta_s y)$ or $\cos(\beta_s y)$, for some constant β_s, we find that the most critical disturbances correspond to $\beta_s = 0$. Hence, we consider $\hat{u}_1$ and $\hat{v}_1$ to be functions of x_s only. Next, multiply the system for $\hat{u}_1$ by $\hat{u}_1$, that for $\hat{v}_1$ by $\hat{v}_1$, add the two results and average over the slow variable x_s. The resulting system then yields the results that no stable solution is possible for sufficiently large h_1, while a stable solution may be possible for sufficiently small h_1 though such a possibility cannot be proved rigorously. It is seen from these results that smaller-R_2 cases are favoured over larger-R_2 cases. Suppose now that $g_1 \neq 0$ and $h_1 = 0$. Then the system for a_1 and b_1 implies that a non-zero value for b_1 is possible for $R_2 > 1$, while R_2 can be smaller for $b_1 = 0$. We find, by assuming $b_1 = 0$, that

$$a_1^2 = 2, \quad R_2 = 2 - g_1/a_1. \tag{3.34}$$

Hence, $a_1 = -\sqrt{2}$ is preferred for $g_1 < 0$, while $a_1 = \sqrt{2}$ is preferred for $g_1 > 0$. The most dangerous disturbances again correspond to the case where $\beta_s = 0$. This result

appears to be general and hold for arbitrary N and $N^{(b)}$. It is due to the fourth-order derivative term in y_s in the systems for $\hat{u}_1$ and $\hat{v}_1$, which leads to a positive constant, and maximizes σ for $\beta_s = 0$. Again forming the integral system for the averaged amplitude of the disturbances, we find that the $b_1 = 0$ solution for (3.34) is stable for $R_2 < 0$. Applying the same method of approach as the one described above for the $g_1 \neq 0$ and $h_1 \neq 0$ case, we find

$$a_1^2 = 1 + b_1^2, \quad R_2 = 2a_1^2 - g_1/a_1, \quad b_1 = a_1 h_1/(g_1 - a_1), \tag{3.35}$$

and this solution is stable for $R_2 < 0$. Again the negative root for a_1 is preferred for $g_1 < 0$, while the opposite is true for $a_1 > 0$.

We now consider the case of arbitrary $N > 1$. Again assuming that the wave vector $\boldsymbol{k}_1$ is along $\boldsymbol{k}_1^{(b)}$, we find from the system for a_n and b_n that a solution exists only for the case where

$$a_n = b_n = 0 \quad \text{for} \quad 1 < n \leqslant N. \tag{3.36}$$

The results given above indicate that small-scale modal roll solutions along the corrugation wave vector $\boldsymbol{k}_1^{(b)}$ with large-scale non-modal roll amplitudes with 'kinks' are preferred. The resulting isotherms at $z = -\frac{1}{2}$ and streamlines in the (x, y)-plane with $\boldsymbol{k}_1^{(b)}$ along the y-axis are shown in figures 2(a) and 2(b) respectively, for $N = N^{(b)} = 1$, $b_1 = h_1 = 0$, $\epsilon = 0.1$, $\alpha = \alpha_n^{(b)} = \pi$ and for a significant imperfection ($\boldsymbol{k}_1 = \boldsymbol{k}_1^{(b)}$). It is seen from these figures that the preferred horizontal flow pattern for $\boldsymbol{k}_1^{(b)}$ is along the y-axis, is periodic in y and symmetric with respect to the y-axis but is non-periodic in x. It represents a pattern due to rectangles near $x = 0$ and rolls parallel to the x-axis for larger $|x|$ which are repeated in the y-direction, but they also vary in x, particularly for small $|x|$. This type of flow pattern may be classified as three-dimensional non-regular mixed rectangles and rolls or a mixed long and short rectangular pattern. The isotherms also exhibit a pattern somewhat similar to that for the horizontal flow structure. The wavenumber in the y-direction is 3.14. The flow is non-periodic along the x-direction.

Example 2

$N^{(b)} = 2$. For significant corrugation effects, we assume $\boldsymbol{k}_1 = \boldsymbol{k}_1^{(b)}$ and $\boldsymbol{k}_2 = \boldsymbol{k}_2^{(b)}$. Consider first $N = 1$. Using the system for a_n and b_n, we obtain the results (3.34) and (3.35) and, thus, the results for the $N^{(b)} = 1$ case (example 1) follow. For $N = 2$, we consider the general case $g_m \neq 0$ and $h_m \neq 0$ ($m = 1, 2$), and we find from the system for a_n and b_n that

$$a_m^2 = (1 + c_{12})^{-1} + b_m^2, \quad b_m = h_m a_m/(g_m - a_m), \quad m = 1, 2, \tag{3.37a}$$

$$R_2 = 2(a_1^2 + c_1 a_2^2) - g_1/a_1 = 2(a_2^2 + c_{12} a_1^2) - g_2/a_2. \tag{3.37b}$$

It is seen from (3.37) and (A) that $c_{ij} > 1$, a negative root for a_m is preferred for $g_1 < 0$, and the opposite is true for $a_m > 0$. Applying the same stability analysis described for example 1, we find that the solution (3.37) is stable for $R_2 < -4(1 + c_{12})[\max(a_1^2, a_2^2)]$.

For $N > 2$ and for significant boundary corrugation where $\boldsymbol{k}_n = \boldsymbol{k}_n^{(b)} (n = 1, 2)$, we find from the system for a_n and b_n that a solution exists only for the case where

$$a_n = b_n = 0 \quad \text{for} \quad 2 < n \leqslant N. \tag{3.38}$$

The results discussed above indicate that the preferred solutions can be either small-scale modal roll solutions with large-scale non-modal roll amplitudes or small-scale modal rectangle-type solutions with larger-scale non-modal amplitude in the form of rectangles. The resulting isotherms at $z = -\frac{1}{2}$ and the flow streamlines in the (x, y)- and

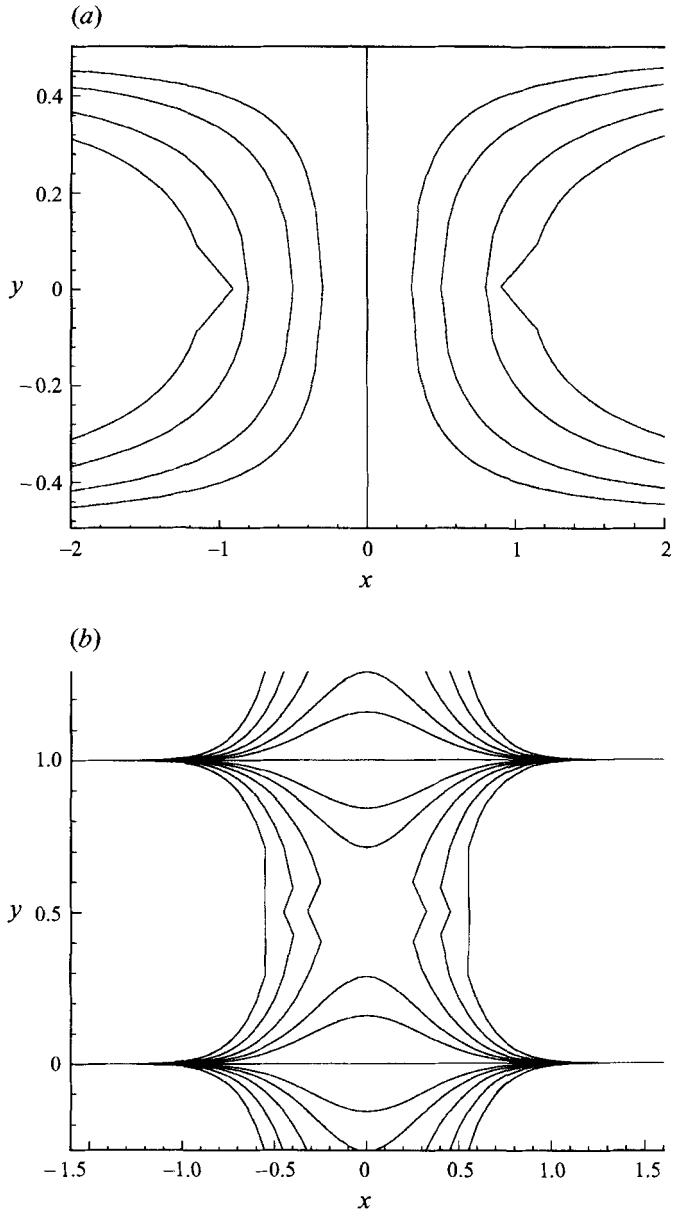

FIGURE 2. (*a*) Isotherms at the lower boundary and (*b*) streamlines in the (x, y)-plane with $\boldsymbol{k}_1^{(b)}$ parallel to y-axis, for $N = N^{(b)} = 1, b_1 = h_1 = 0, \epsilon = 0.1, \boldsymbol{k}_n = \boldsymbol{k}_n^{(b)}, \alpha = \alpha_n^{(b)} = \pi$.

(x, z)-planes are determined for $N = N^{(b)} = 1$, $b_n = h_n = 0$, $\boldsymbol{k}_n = \boldsymbol{k}_n^{(b)} (n = 1, 2)$, $g_1 = g_2$, $\epsilon = 0.14$, $\alpha = \alpha_n^{(b)} = \pi$ and for $\boldsymbol{k}_1^{(b)} + \boldsymbol{k}_2^{(b)}$ parallel to the x-axis and $\boldsymbol{k}_1^{(b)} - \boldsymbol{k}_2^{(b)}$ parallel to the y-axis. It is found from these results that the preferred horizontal and vertical flow patterns are similar, in the form of non-regular and non-periodic rectangles for small $|x|$ near $x = 0$ which changes to regular squares for sufficiently large $|x|$. The boundary imperfection isotherms display a similar x-dependent pattern with a sharp change in the pattern across the y-axis ($x = 0$). The wavenumber in the y-direction is 3.14. The flow is non-periodic with respect to x, but is periodic in y.

The two examples presented above can be generalized to arbitrary $N^{(b)}$. The preferred flow solution is a superposition of a small-scale multi-modal ($N \leqslant N^{(b)}$) solution and a large-scale multi-non-modal ($N \leqslant N^{(b)}$) amplitude function.

4. Non-resonant wavelength excitation

4.1. *General analysis*

This case corresponds to the critical regime where $R \approx R_c$ and it turns out, as we showed in Riahi (1993), that $O(\epsilon^2) < \delta < O(\epsilon)$. Following Pal & Kelly (1978) and Riahi (1993), we consider the following expressions for ϕ, θ and R in powers of ϵ and δ:

$$\begin{pmatrix} \phi \\ \theta \\ R \end{pmatrix} = \sum_{m=0} \sum_{n=0} \epsilon^m \delta^n \begin{pmatrix} \phi_{mn} \\ \theta_{mn} \\ R_{mn} \end{pmatrix}; \quad \phi_{00} = \theta_{00} = 0. \tag{4.1}$$

Upon inserting (4.1) into (2.3*b*, *c*), (2.5) and (2.6) and disregarding the quadratic terms, we find the linear problem whose order-$\epsilon^1 \delta^0$ system is of the form given in Riahi (1993). The solution to this system can be written in the form (3.2), provided ϕ_1 and θ_1 are replaced, respectively, by ϕ_{10} and θ_{10}.

The order $\epsilon^0 \delta^1$ system of the linear problem is of the form given in Riahi (1993) whose solution can be written as

$$\begin{pmatrix} \phi_{01} \\ \theta_{01} \end{pmatrix} = \sum_{n=-N^{(b)}}^{N^{(b)}} L_n \begin{pmatrix} f_n(z) \\ g_n(z) \end{pmatrix} w_n^{(b)}, \tag{4.2}$$

where the system and the solution for f_n and g_n are given in Riahi (1993). As was noted in Riahi (1993), the double-series expansion procedure of this section breaks down for $\alpha_n^{(b)} = \alpha_c$ since g_n and f_n become unbounded. Hence, our method of solution here is strictly valid for $\alpha_n^{(b)} \neq \alpha_c$.

Some results presented in Riahi (1993) indicated that

$$O(\epsilon^2) < \delta < O(\epsilon), \tag{4.3}$$

which holds in the present problem as well. This result implies the need for an expression for R_{01} which is found by applying the solvability condition and averaging in x, y and z for the order-ϵ δ system of the nonlinear problem. Using (4.2), this condition can be simplified to the following form:

$$A_n^* R_{01} = \sum_{lp} L_p S_{lp} < w_n w_l w_p^{(b)} > A_l \quad (n = -N, \ldots, -1, 1, \ldots, N), \tag{4.4}$$

where the expression for the coefficient S_{lp}, which is a function of $\alpha_p^{(b)}$ and $\phi_{1p}^{(b)}$, is given in Riahi (1993) and

$$\phi_{1p}^{(b)} = (\boldsymbol{k}_1 \cdot \boldsymbol{k}_p^{(b)})/(\pi \alpha_p^{(b)}).$$

It can be seen from (4.4) that R_{01} can be non-zero if

$$\boldsymbol{k}_n + \boldsymbol{k}_l + \boldsymbol{k}_p^{(b)} = 0 \tag{4.5}$$

for at least some values of l and p. However, for $\alpha_p^{(b)} = 2\pi$, R_{01} is zero even if (4.5) is satisfied since S_{1p} vanishes (Riahi 1993). Using (3.6), (3.8) and following the same procedure and analysis as discussed in Riahi (1993), we find that non-trivial results due to significant boundary modulations exist only if

$$\alpha_p^{(b)} < 2\pi \tag{4.6}$$

for at least some p. We shall assume that the condition given by (4.6) is valid. Such a condition can also be inferred from the order-$\epsilon\,\delta$ system with resonant terms treated by Rees & Riley (1989*b*).

4.2. *Modal analysis*

Using (3.11) and (3.14) in (4.4), multiply the resulting system (4.4) by $v_{n'n}$ and average over the slow variables, we end up with a system for the coefficients $a_{nn'}$. This system turns out to imply that the expression for the product $R_{01}\,a_{nn'}$ can be non-zero only if (4.6) and the condition

$$\gamma_{jp}^{(b)}+\gamma_{m'l}+\gamma_{n'n}=0 \tag{4.7}$$

hold for at least some j and m' and a given n'. The condition (4.7) holds only if the three wave vectors γ_{jp}, $\gamma_{m'l}$ and $\gamma_{n'n}$ form a triangle so that the component of the flow pattern due to amplitude functions can be rectangular cells.

Let us now consider the following specific examples based on the system for $a_{nn'}$ in order to illustrate the non-trivial and often surprising inter-relations between the boundary modulation pattern and the subsequent preferred flow pattern.

Example 1

$M^{(b)}=N^{(b)}=1$, $\pi\neq\alpha_m^{(b)}<2\pi$ and all the $\alpha_m^{(b)}$ have the same value. The expression for $R_{01}\,\alpha_{nn'}$ can be non-zero only if (4.5) and (4.7) hold and if

$$\phi_{lp}^{(b)}=\phi_{np}^{(b)}=\alpha_p^{(b)}/(2\pi)\quad\text{and}\quad\lambda^{(b)}<2\lambda. \tag{4.8}$$

This result implies that the preferred flow solution is of a small-scale rectangular type where the angle w between two adjacent wave vectors is either

$$w=2\cos^{-1}[\alpha_p^{(b)}/(2\pi)]\quad\text{or}\quad 180^\circ-w, \tag{4.9}$$

and a large-scale rectangular shaped amplitude. For $\alpha_p^{(b)}=\sqrt{2}\,\pi$, a small-scale square solution and a large-scale rectangular-type amplitude is preferred. Since $\alpha_p^{(b)}\neq 0$, a small-scale two-dimensional roll pattern is not possible. The preferred rectangular-type amplitude depends on the initial conditions since the angle between two adjacent γ_{1m} vectors is arbitrary.

The streamlines in the (x,y)-plane are shown in figure 3 for $N^{(b)}=M^{(b)}=1$, $N=M=2$, $\pi\neq\alpha_m^{(b)}<2\pi$, $\lambda^{(b)}<\lambda=\pi$, $\alpha=\pi$, $\epsilon=0.1$, $l_{11}=l_{1,-1}=l_{-1,-1}$, with $\boldsymbol{k}_1$ and $\gamma_{11}^{(b)}$ parallel to the x-axis, $\boldsymbol{k}_2$ and γ_{22} parallel to the y-axis, and $\boldsymbol{k}_1^{(b)}$ and $\gamma_{11}^{(b)}$ parallel to the line $y=-x$. Also, the sign of l_{11} is chosen such that $l_{11}\,S_{11}<0$. The isotherms for this case are not presented in the figure since they are simple straight lines parallel to $y=-x$. It is seen from figure 3 that the preferred horizontal flow pattern exhibits a double cell structure. There are large square cells, repeated every 10 units in the x- and y-directions, and there are also small square cells which are repeated every $\sqrt{2}$ units along the boundaries of the large cells (parallel to lines $y=\pm x$).

Example 2

$M^{(b)}\leqslant 2$, $N^{(b)}=2$, $\pi\neq\alpha_m^{(b)}<2\pi$ and all the $\alpha_m^{(b)}$ have the same value. We find that a small-scale square-type solution with large-scale amplitude in the form of rectangular ($M^{(b)}\leqslant 2$) or multi-modal ($M=4$, $M^{(b)}=2$) pattern is preferred for $\alpha_m^{(b)}=\sqrt{2}\,\pi$. For other values of $\alpha_m^{(b)}$, a small-scale rectangular ($M^{(b)}\leqslant 2$) or multi-modal ($N=4$, $M^{(b)}=2$) type solution with large-scale rectangular ($M^{(b)}\leqslant 2$) or multi-modal ($M=4$, $M^{(b)}=2$) amplitude with an arbitrary γ_{1m} orientation is a possible preferred solution leading to the same critical R_{01}, and thus the solution realized is the one due to the initial condition. For $\lambda=\lambda^{(b)}/\sqrt{2}$, these results are valid, provided that the large-scale

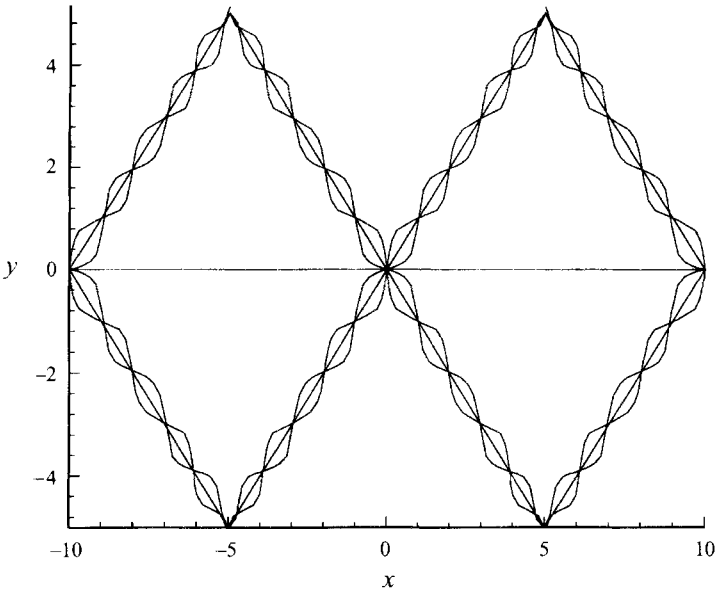

FIGURE 3. Streamlines in the (x, y)-plane for $N^{(b)} = M^{(b)} = 1, N = M = 2, \alpha_m^{(b)} \equiv \alpha^{(b)}, \pi \neq \alpha^{(b)} < 2\pi$, $\lambda^{(b)} < \lambda, \epsilon = 0.1, \lambda = \pi, \alpha = \pi, l_{11} = l_{1,-1} = l_{-1,-1}$, with $\boldsymbol{k}_1$ and γ_{11} parallel to the x-axis, $\boldsymbol{k}_2$ and γ_{22} parallel to the y-axis, and $\boldsymbol{k}_1^{(b)}$ and $\gamma_{11}^{(b)}$ parallel to the line $y = -x$. The sign of l_{11} is chosen such that $l_{11} S_{11} < 0$.

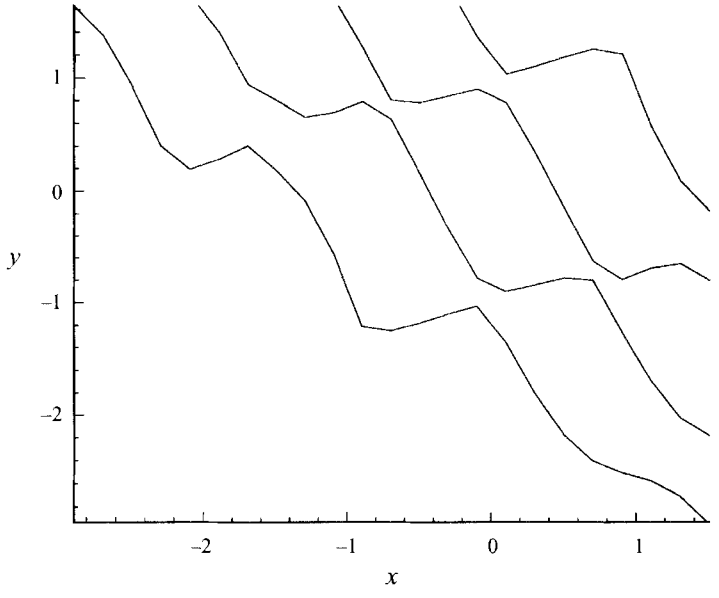

FIGURE 4. Isotherms at the lower boundary for $M^{(b)} = 1, N^{(b)} = 2, \lambda^{(b)} = \alpha_m^{(b)} = \sqrt{2}\pi, \epsilon = 0.1, l_{11} = l_{1,-1}$, with $\boldsymbol{k}_1^{(b)}$ and $\gamma_{11}^{(b)}$ parallel to line the $y = -x, \boldsymbol{k}_2^{(b)}$ paralle to the x-axis and $\gamma_{12}^{(b)}$ parallel to the y-axis.

rectangular amplitude is replaced by a large-scale amplitude in the form of squares. The isotherms at $z = -\frac{1}{2}$ are shown in figure 4 for $M^{(b)} = 1$, $N^{(b)} = 2$, $\alpha_m^{(b)} = \lambda^{(b)} = \sqrt{2}\pi$, $\epsilon = 0.1$, $l_{11} = l_{1,-1}$, *with* $\boldsymbol{k}_1^{(b)}$ and $\gamma_{11}^{(b)}$ parallel to the line $y = -x$, $\boldsymbol{k}_2^{(b)}$ parallel to the x-axis and $\gamma_{12}^{(b)}$ parallel to the y-axis. It is seen from this figure that isotherms form

a pattern similar to that due to a semi-regular rectangle. The averaged direction of the isotherms is close to that of the line $y = -x$. The flow streamlines for this case have the same form as those shown in figure 3.

The above examples can be extended to arbitrary $N^{(b)}$ and $M^{(b)}$. For $\gamma^{(b)}_{m'p} \cdot \gamma^{(b)}_{p'm} = 0$ and $k^{(b)}_m \cdot k^{(b)}_p = 0$ hold j' and j integers numbers of times, respectively, and for $R_{01} < 0$, large-scale multi-modal ($M = 2, \ldots, 2j'$) amplitudes superimposed on small-scale multi-modal ($N = 2, \ldots, 2j$) solutions are all possibly preferred for $\alpha^{(b)}_m = \sqrt{2}\pi$. For $R_{01} > 0$, large- and small-scale forms are replaced by large- and small-scale multi-modal ($M = 2, \ldots, 2(M^b - J')$) and ($N = 2, \ldots, 2(N^{(b)} - J)$) forms respectively. For all other cases, large- and small-scale forms are replaced by multi-modal ($2 \leqslant M \leqslant 2M^{(b)}$) and ($2 \leqslant N \leqslant 2N^{(b)}$) forms, respectively, with arbitrary γ_{1n} orientations, leading to the same critical R_{01}, and thus the preferred solution is one of these due to the initial condition.

4.3. *Non-modal analysis*

We consider the system (4.4) for this analysis. Taking the complex conjugate of (4.4) and using it back in (4.4) leads to a linear algebraic system for $A_n (n = -N, \ldots, -1, 1, \ldots, N)$. The boundary imperfection functions $L_p (P = -N^{(b)}, \ldots, -1, 1, \ldots, N^{(b)})$ are assumed to be given. The system for A_n then has, in general, non-trivial solutions for A_n, provided the determinant of the coefficients of the unknowns A_n vanishes. This leads to an equation for $L^*_p L p_1 (p, p_1 = -N^{(b)}, \ldots, -1, 1, \ldots, N^{(b)})$ which must be satisfied by the functions L_p. The amplitude functions A_n can then be determined from the system for A_n, which are all but one affected by L_p. Only one of the functions A_n can be chosen arbitrarily owing to the linearity of the amplitude system with respect to A_n. Therefore, in general, the large-scale amplitude of the resulting flow solution(s) should depend on the boundary imperfections.

Since L_p are, in general, functions of the slow variables, the above-stated determinant equation can be satisfied when L_p is given by

$$L_p = g_p(\tanh x_s + \mathrm{i}(p/|p|)\,\mathrm{sech}\, x_s), \tag{4.10}$$

where the g_p are some real constants. Such a form for the boundary imperfection functions L_p is suggested by the system for A_n and the above analysis and can lead to the unusual non-modal solutions for a 'kink' that were predicated in §3.3.

Let us now consider the following specific examples based on the system for A_n in order to illustrate the inter-relations between the boundary imperfections and the resulting flow solution.

Example 1

$N^{(b)} = 1$ and $\pi \neq \alpha^{(b)}_p < 2\pi$. The expression for $R_{01} a_{nn'}$ in the system for A_n can be non-zero only if (4.5) holds and if

$$\phi^{(b)}_{lp} = \phi^{(b)}_{np} = \phi^{(b)}_{lp_1} = \phi^{(b)}_{l_1 p_1} = \alpha^{(b)}_p/(2\pi) \tag{4.11}$$

for at least some values of the subscripts. This result implies that only $N = 2$ is possible. Using the system for A_n and (4.10) and (4.11), we obtain

$$R_{01} = \pm|g_1 S_{11}|, \quad A_1 R_{01} = g_1 S_{11}(\tanh x_s - \mathrm{i}\,\mathrm{sech}\, x_s) A^*. \tag{4.12}$$

It is seen from (4.12) that both supercritical ($R_{01} > 0$) and subcritical ($R_{01} < 0$) solutions are possible, but the preferred solution corresponds to $R_{01} < 0$. The results discussed above imply that the preferred flow solution is made up of a small-scale modal rectangular-type solution, where the angle w between two adjacent wave vectors

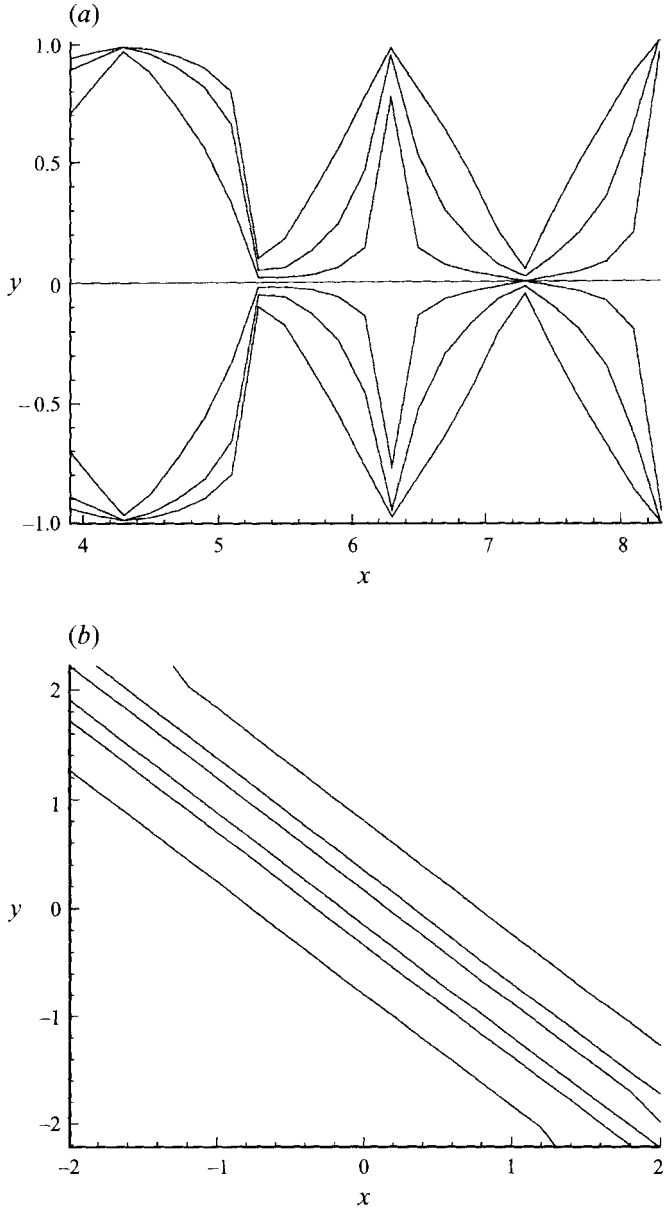

FIGURE 5. (*a*) Streamlines in the (x, y)-plane and (*b*) isotherms at the lower boundary, for $N = 2, N^{(b)} = 1, \alpha = \pi, \alpha_m^{(b)} = \sqrt{2}\pi, \epsilon = 0.1$, and for $\boldsymbol{k}_1$ parallel to the x-axis, $\boldsymbol{k}_2$ parallel to the y-axis, and $\boldsymbol{k}_1^{(b)}$ parallel to line the $y = -x$.

satisfies (4.9), and a large-scale non-modal rectangular-type amplitude with a 'kink'. The resulting streamlines in the (x, y)-plane and the isotherms at $z = -\frac{1}{2}$ are shown, respectively, in figures 5(*a*) and 5(*b*) for $N = 2, N^{(b)} = 1, \alpha = \pi, \alpha_m^{(b)} = \sqrt{2}\pi, \epsilon = 0.1$, and for $\boldsymbol{k}_1$ parallel to the x-axis, $\boldsymbol{k}_2$ parallel to the y-axis and $\boldsymbol{k}_1^{(b)}$ parallel to the line $y = -x$. The coefficient g_1 is chosen such that arbitrarily A_2 takes the value -1. The results shown in these figures indicate that the flow streamlines represent a pattern close to that of irregular rectangles. The isotherms indicate a pattern close to that of somewhat irregular rolls inclined primarily in the direction of $y = -x$. The horizontal

flow structure and the imperfection isotherms are periodic in y but non-periodic in x, unless $|x| \to \infty$.

Example 2

$N^{(b)} = 2, \pi \neq \alpha_m^{(b)} < 2\pi$ and all the $\alpha_m^{(b)}$ have the same magnitude. We also assume that the distribution of $\boldsymbol{k}_m^{(b)}$ vectors is regular. We find that the small-scale modal square solution with a large-scale non-modal rectangular amplitude with a 'kink' is preferred for $\alpha_m^{(b)} = \sqrt{2\pi}$. For other values of $\alpha_m^{(b)}$, either a small-scale modal rectangular solution with a large-scale non-modal rectangular amplitude with a 'kink' or a small-scale multi-modal ($N = 4$) solution with a large – scale multi-non-modal ($N = 4$) amplitude with a 'kink' is a possible preferred flow solution. The resulting streamlines in the (x, y)-plane and the isotherms at $z = -\frac{1}{2}$ are determined for $N = N^{(b)} = 2, \alpha = \pi$, $\alpha_m^{(b)} = \sqrt{2\pi}, \epsilon = 0.1, g_1 = g_2$, and for $\boldsymbol{k}_1$ parallel to the x-axis, $\boldsymbol{k}_2$ and $\boldsymbol{k}_2^{(b)}$ parallel to the y-axis and $\boldsymbol{k}_1^{(b)}$ parallel to the line $y = -x$. The coefficient g_2 is chosen such that $R_{01} = g_2 S_{21}^* < 0$. The arbitrary amplitude A_2 is chosen to be the inverse of $\cos(\pi y)$. The results indicate that the flow streamlines represent a pattern close to that for an irregular rectangle. The isotherms indicate a pattern close to that for a different irregular rectangle. The horizontal flow structure and the isotherms are periodic in y but are non-periodic in x, unless $|x|$ is sufficiently large.

The above examples can be extended to arbitrary $N^{(b)}$ and for a regular distribution of $\boldsymbol{k}_m^{(b)}$. For the case where $\boldsymbol{k}_m^{(b)} \cdot \boldsymbol{k}_p^{(b)} = 0$ holds j integer number of times and for $R_{01} < 0$, the large-scale multi-non-modal ($N = N_1$) amplitude superimposed on the small-scale multi-modal ($N = N_1$) solution is preferred for each $N_1 (N_1 = 2, \ldots, 2j)$ for $\alpha_m^{(b)} = \sqrt{2\pi}$. For $R_{01} > 0$, large- and small-scale solutions are replaced by a large-scale multi-non-modal ($N = N_2$) and small-scale multi-modal ($N = N_2$) solution for each $N_2 (N_2 = 2, \ldots, 2(N^b - j))$. For other cases, large- and small-scale solutions are replaced by a multi-non-modal ($N = N_3$) and a multi-modal ($N = N_3$) solution, respectively, for each $N_3 (N_3 = 2, \ldots, 2N^{(b)})$.

5. Discussion

As was shown in Riahi (1993) and also turns out to be true in the present case, the present problem does not lead to qualitatively different results from those for the problem where the lower boundary's location is at $z = -\frac{1}{2} + \delta h(x, y)$, and the boundary corrugated problem can incorporate the effects of roughness elements of arbitrary shape h, provided that $N^{(b)}$ can tend to infinity and that $\alpha_m^{(b)}$ do not all have the same value. The discussion presented in Riahi (1993) can be extended to the present problem which indicates that the results presented in §3 are valid for terms in (3.8) for h with $\alpha_n^{(b)} = \pi$, the results presented in §4 are valid for terms in (3.8) with $2\pi > \alpha_n^{(b)} \neq \pi$, and the terms in (3.8) with $2\pi < \alpha_n^{(b)}$ make zero contribution to various flow features and are irrelevant for the present problem.

Rees & Riley (1986) considered thermal convection rolls in a porous medium between two one-dimensional undulating boundaries. They found that boundary modulation effects can be stabilizing. Later the same authors (Rees & Riley 1989*a*, *b*) investigated the effects of a simple sinusoidal boundary imperfection on weakly nonlinear convection. They determined the equation for the flow amplitude and investigated two-dimensional rolls solutions. Then, the stability of one or two sets of rolls solutions with respect to different roll disturbances were studied. They found, in particular, that the region of linear stability of the rolls is enlarged by the presence of the modulations. For a wide range of modulation wavenumber a three-dimensional

motion with a rectangular panform results from a resonant interaction between a pair of oblique rolls and the boundary forcing. Their results generally agree with the modal case of the present results for $N^{(b)} = 1$ and with (3.27).

The problem studied in the present paper deals with convection in a horizontal layer bounded by plates whose mean temperatures are maintained at constant values. This problem, as Newell & Whitehead (1969) demonstrated, has the property that it admits slow horizontal variables x_s and y_s of orders ϵ and $\epsilon^{1/2}$, respectively, and x_s dependence is more important than y_s dependence. This property is due to the fact that for R just beyond R_c, in the absence of boundary imperfections, two-dimensional rolls are preferred (Newell & Whitehead 1969; Riahi 1983), where it is assumed that the x-axis is along these rolls. The resulting amplitude system (A) is then a system of partial differential equations where each equation is second order in derivatives with respect to x_s and fourth order in derivatives with respect to y_s. Another equally important problem, with possible geothermal applications, is convection in a horizontal layer bounded by two poorly conducting plates. It can then be shown easily that such a problem admits the slow variables x_s and y_s which are now both of order ϵ, and x_s dependence and y_s dependence are equally important. This property is due to the fact that for R just beyond R_c, in the absence of boundary imperfections, three-dimensional solutions in the form of squares are preferred (Riahi 1983). The resulting amplitude system will then be a system of partial differential equations where each equation is second order in derivatives with respect to both x_s and y_s. Although the results for such system will be reported elsewhere, it is of interest to note here that such a system can admit non-modal solutions with kinks, different from those discussed in the present paper, and the resulting preferred patterns will be affected accordingly.

Another interesting extension of the present study, to be considered in a future contribution, is to investigate temporal imperfection effects in order to explore the possibilities for the preference of new patterns with temporal kinks. However, such an extension should be carried out for convection systems where time-dependent solutions can be preferred since it has been shown recently (Riahi 1995), for simple temporal or one-dimensional spatial sinusoidal boundary modulation effects on convection in a rotating system, that the spatial or temporal type of modulation mode is effective only if it is acceptable to the linear system. For example, the oscillatory mode of modulation is found to be ineffective for the case where the linear theory predicts that the steady solutions are preferred.

Although there have been very few studies so far on the problems of modal package convection or problems of convection influenced by boundary imperfections, the importance of such problems cannot be underestimated. Modal package convection provides a larger manifold of realizable patterns due to solutions as the result of external forcing or from general initial and boundary conditions. Closely compatible with such systems are convection systems of the type considered in the present paper which provide, in addition to a larger manifold of realizable patterns, a way to control instabilities and flow structures.

6. Conclusions

The results of the present study lead to the following conclusions.

(i) Depending on the values of the wavenumbers involved, the flow structure may or may not be repeatable in the horizontal direction.

(ii) The preferred flow pattern resembles quite closely the isothermal pattern due to boundary imperfections for near-resonant wavelength excitation. For non-resonant

wavelength excitation, the preferred flow pattern is, generally, quite different from the isothermal pattern due to the boundary imperfections.

(iii) The wavenumbers of the modal components of the preferred flow solution are, generally, different from the classical ones.

(iv) The preferred flow pattern is, generally, more regular for the case of the modal form of boundary imperfections, while it is, generally, more non-regular and three-dimensional for the non-modal form of the boundary imperfections.

(v) The preferred flow solution is, generally, non-periodic with respect to x for the non-modal form of boundary imperfections.

(vi) The preferred flow pattern is, mostly, a multiple of rectangular patterns.

(vii) The boundary imperfections can have profound non-trivial effects on the flow patterns realized, leading to the preference for a certain continuous finite bandwidth of modes which may not be realized by other means.

(viii) The preference for solutions with either a modal or non-modal form of the amplitude functions representing a continuous finite bandwidth of convection modes was demonstrated and a wider class of solutions which can be both realizable and stable only in the presence of boundary imperfections was obtained.

The author would like to thank the referees for useful and constructive suggestions which led to the improvement of the paper.

REFERENCES

JOSEPH, D. D. 1976 *Stability of Fluid Motions*, vols. I and II. Springer.

KELLY, R. E. & PAL, D. 1976 Thermal convection induced between non-uniformity heated horizontal surfaces. *Proc. Heat Transfer and Fluid Mech. Inst.*, pp. 1–17. Stanford University Press.

KELLY, R. E. & PAL. D. 1978 Thermal convection with spatially periodic boundary conditions: resonant wavelength excitation. *J. Fluid Mech.* **86**, 433–456.

NEWELL, A. C. & WHITEHEAD, J. A. 1969 Finite bandwidth finite amplitude convection. *J. Fluid Mech.* **39**, 279–303.

PAL, D. & KELLY, R. E. 1978 Thermal convection with spatially periodic nonuniform heating: nonresonant wavelength excitation. *Proc. 6th Intl. Heat Transfer Conf. Toronto*, pp. 235–238.

REES, D. A. S. & RILEY, D. S. 1986 Free convection in an undulating saturated porous layer: Resonant wavelength excitation. *J. Fluid Mech.* **166**, 503–530.

REES, D. A. S. & RILEY, D. S. 1989*a* The effects of boundary imperfections on convection in a saturated porous layer: near-resonant wavelength excitation. *J. Fluid Mech.* **199**, 133–154.

REES, D. A. S. & RILEY, D. S. 1989*b* The effects of boundary imperfections on convection in a saturated porous layer: non-resonant wavelength excitation. *Proc. R. Soc. Lond.* A **421**, 303–339.

RIAHI, D. N. 1983 Nonlinear convection in a porous layer with finite conducting boundaries. *J. Fluid Mech.* **129**, 153–171.

RIAHI, D. N. 1993 Preferred pattern of convection in a porous layer with a spatially non-uniform boundary temperature. *J. Fluid Mech.* **246**, 529–543.

RIAHI, D. N. 1995 Nonlinear instabilities of steady and oscillatory wave convection in a rotating system. *Proc. First World Cong. Nonliner Analysis, Tampa, FL Aug. 1992*, in press.